JOURNAL OF SOLID STATE CHEMISTRY **124,** 58–64 (1996)
ARTICLE NO. 0207

The Structure of Tantalum Tungsten Oxide $Ta_8W_9O_{47}$

Frank Krumeich[1] and Thomas Geipel

Institut für Anorganische Chemie der Universität Bonn, Römerstrasse 164, D-53117 Bonn, Germany

Received October 24, 1995; in revised form February 21, 1996; accepted February 29, 1996

The TTB-type (tetragonal tungsten bronze) structure of $Ta_8W_9O_{47}$ has been investigated for two different processing temperatures (T = 1200 and 1400°C) using X-ray powder diffraction and TEM methods. The Guinier patterns for both temperatures show the reflections of the TTB-type structure. Additionally, the product obtained at 1400°C exhibits the reflections of a threefold TTB-type superstructure. HRTEM images of this specimen (along [001]) show that the superstructure originates from a systematic arrangement of PCs (pentagonal columns) in the TTB-type framework which is also known from $Nb_8W_9O_{47}$. For 1200°C, the electron diffracton patterns (along [001]) exhibit circular diffuse scattering around the basic reflections and additional superstructure reflections can be observed at the intersections of the circles with both tetragonal axes. A structural model for the low-temperature phase has been derived from HRTEM images. It is shown (using Fourier analysis) that the diffuse scattering is caused by a disordered distribution of the PCs. In case of a locally incomplete reaction, the arising defect structure of a tungsten-rich crystal area is characterized using HRTEM.

1. INTRODUCTION

In the pseudo-binary system Ta_2O_5/WO_3, various kinds of structures are known: In the tungsten-rich region with an oxygen to metal ratio $O/\Sigma M > 2.9$ (M = Ta, W), the Magnéli phases (CS structures) occur (1–4). They are derived from the ReO_3 type which consists of corner-sharing ReO_6 octahedra arranged on a primitive cubic lattice. Starting with WO_3 ($O/\Sigma M = 3$), the reaction with Ta_2O_5 leads to decreased $O/\Sigma M$-ratios structurally accommodated by introduction of edge-sharing between octahedra (crystallographic shear, CS). In the tantalum-rich part of the system ($O/\Sigma M < 2.67$), the so-called adaptive structures have been observed (5–9) which are (as well as the related L-Ta_2O_5 (10)) superstructures of the basic U_3O_8 type. In the medium region, Ta_2WO_8 (11) crystallizes in the $LiNb_6O_{15}F$-type structure (12). The structures of tantalum tungsten oxides with compositions between Ta_2WO_8 and the Magnéli phases are of the TTB (tetragonal tungsten bronze) type. $Ta_4W_7O_{31}$ exibits an intergrowth structure between TTB and ReO_3 type (4). Besides that, a pyrochlore-type structure was found for a composition $TaWO_{5,5}$ (13).

Depending on composition and preparation conditions, the TTB-type phases are tetragonal or have a threefold superstructure leading to an orthorhombic unit cell. In the TTB structure, corner-sharing octahedra are arranged to build five-membered rings. In the direction of the short crystallographic axis, the octahedra share their corners which gives rise to pentagonal tunnels; four of them are present in the unit cell of the TTB structure arranged around a central square of octahedra.

In the system Nb_2O_5/WO_3, the structurally well-characterized 4:9 phase ($Nb_8W_9O_{47}$) (14) crystallizes in a threefold TTB-type superstructure caused by the systematic occupation of 1/3 of the pentagonal tunnels with metal–oxygen strings. The coordination of these cations are pentagonal bipyramids which are connected to five equatorial MO_6 octahedra each leading to the so-called PCs (pentagonal columns (15)). In this structure, twinning with the twinning plane being (130) (14, 16) occurs frequently. Niobium tungsten oxides with compositions between the 4:9 phase ((Nb, W)$O_{2.765}$) and the 2:7 phase ((Nb, W)$O_{2.818}$) exhibit a disordered distribution of the PCs leading to diffuse scattering (17-19).

In case of $Ta_8W_9O_{47}$, only X-ray powder diffraction experiments have been performed by several authors up to now. For this composition, two variants with either tetragonal or orthorhombic unit cells have been found (Table 1). In this paper, electron diffraction and HRTEM (high-resolution transmission electron microscopy) have been applied in order to characterize the structures of both variants of $Ta_8W_9O_{47}$.

2. EXPERIMENTAL

Mixtures of Ta_2O_5 (99,99%, Aldrich) and WO_3 (extra pure, Riedel-de-Haën) in the molar ratio 4:9 have been annealed in sealed platinum ampoules in ambient air

[1] Present address: Institut für Angewandte Chemie Berlin-Adlershof, Rudower Chaussee 5, D-12484 Berlin, Germany.

0022-4596/96 $18.00

TABLE 1
Lattice Parameters of $Ta_8W_9O_{47}$

a (nm)	*b* (nm)	*c* (nm)	Preparation	References
1.2257	3.6298	0.3886	Ta_2O_5:WO_3 = 1:2, T = 1370°C	[14]
1.2266	3.6274	0.3886	Ta_2O_5:WO_3 = 1:3, T = 1400°C	[14]
1.224(1)	3.660(1)	0.3877(3)	T = 1100°C	[1]
1.2251(1)		0.3882	T = 1350°C	[20]
1.225(7)	3.627(9)	0.388(6)	Pyrolysis	[21]
1.2284(2)	3.6697(5)	0.38896(7)	T = 1400°C	This work
1.2248(1)		0.38842(6)	T = 1200°C	This work

(T = 1200°C, 60 h and T = 1400°C, 120 h). The lattice parameters of the products were determined from X-ray powder diffraction patterns (Guinier method, λ = 0.15405 nm).

For TEM investigation (Philips CM30ST electron microscope), the samples were ground in an agate mortar and dispersed in acetone. A few droplets were brought onto a perforated Formvar foil (carbon coated) supported by a copper grid. The ratios Ta/W of the investigated crystals have been determined to be 8/9 by EDX analyses (Tracor Voyager system, Ge detector) indicating a complete reaction leading to the atomic composition $Ta_8W_9O_{47}$. HRTEM images have been recorded near Scherzer focus so that the positions of the metal atoms appear as dark dots (22). In the present structure, the polyhedra are connected by corner-sharing to form columns in the direction of the short crystallographic axis (c-axis) which are observed in the [001] direction.

The HRTEM negatives have been scanned using a high-resolution drum scanner (Optotech) allowing digital image processing which has been performed using the programming language IDL.

3. RESULTS AND DISCUSSION

Orthorhombic $Ta_8W_9O_{47}$ (T = 1400°C)

The Guinier diagram (Fig. 1b) and the electron diffraction pattern along [001] (inset in Fig. 2) reveal the reflections of the threefold TTB-type superstructure. The corresponding lattice parameters of the orthorhombic unit cell coincide with preceding investigations (Table 1). A typical HRTEM image (Fig. 2) exhibits the presence of the ideal structure in a large crystal region. In Fig. 3, the enlargement of a part of Fig. 2 shows that the superstructure results from the systematic distribution of PCs (pentagonal columns) in the TTB-type framework. The PCs appear as centered pentagons of dark dots. The observed cation arrangement is identical to that found for $Nb_8W_9O_{47}$ (14) resulting in similar HRTEM images (23, 24). In this structure, two PCs are connected via a common square of octahedra (diamond link (25)). Two kinds of these pairs occur in different orientations.

The local occupation ratio Ta/W on the cation sites can not be determined using HRTEM. In case of $Nb_8W_9O_{47}$, the cation site with pentagonal bipyramidal coordination is occupied by Nb atoms preferentially which has been shown using X-ray diffraction on single-crystals (14). Possibly, this is also the case for Ta since this coordination is preferred in tantalum oxides (10).

Tetragonal $Ta_8W_9O_{47}$ (T = 1200°C)

The Guinier diagram (Fig. 1a) of the low-temperature product exhibits only the reflections of the tetragonal TTB-type subcell. The corresponding lattice parameters are given in Table 1.

Further structural information about this sample can be obtained using TEM. The electron diffraction pattern (along [001], Fig. 4) exhibits the reflections of the TTB-type structure and circular diffuse scattering which occurs around each spot. The radii of the circles correspond to $\frac{1}{3}$ of the distance between the main spots ($\frac{1}{3}\langle 100\rangle^*$). At the intersections with the tetragonal axes, they appear brighter. These positions in reciprocal space correspond to the reflections of the threefold TTB-type superstructure present in the high-temperature structure (Fig. 2). The lattice image (Fig. 4) shows that the threefold TTB-type structure is present in small domains as can be seen from the distribution of PCs outlined in Fig. 5a and Fig. 6a, respectively. Two perpendicular orientations of these microdomains exist giving rise to the superstruc-

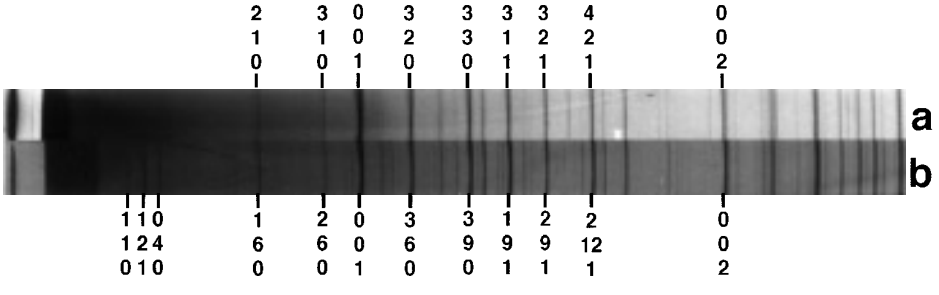

FIG. 1. Guinier patterns of $Ta_8W_9O_{47}$ prepared at (a) T = 1200°C and (b) T = 1400°C with indices of the main reflections.

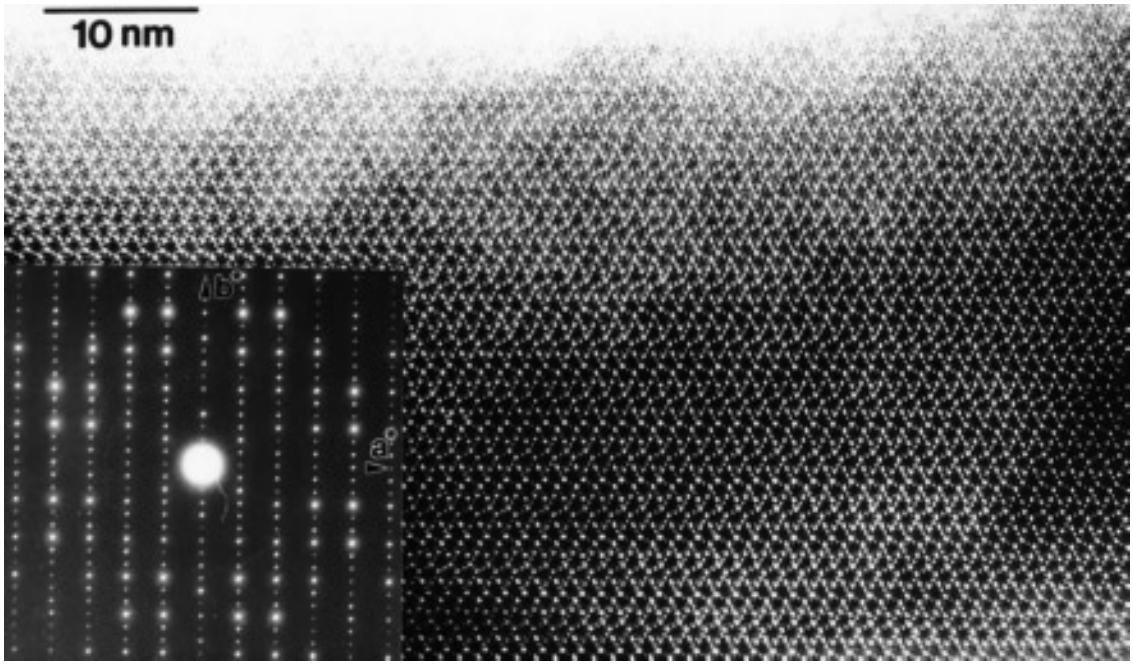

FIG. 2. $Ta_8W_9O_{47}$ (T = 1400°C): HRTEM image and electron diffraction pattern along [001].

ture reflections along both axes of the tetragonal substructure. This corresponds to the twinned orthorhombic structure with the twinning plane being (130). The areas between these ordered domains contain an almost undisturbed framework of the TTB-type substructure but a disordered distribution of PCs. Either isolated PCs or chains of PCs are observed (Fig. 5a, 6a). In these chains, which are up to nine PC elements long, PCs are connected via a common square of octahedra (diamond link). They occur along two directions: Every pentagon of octahedra

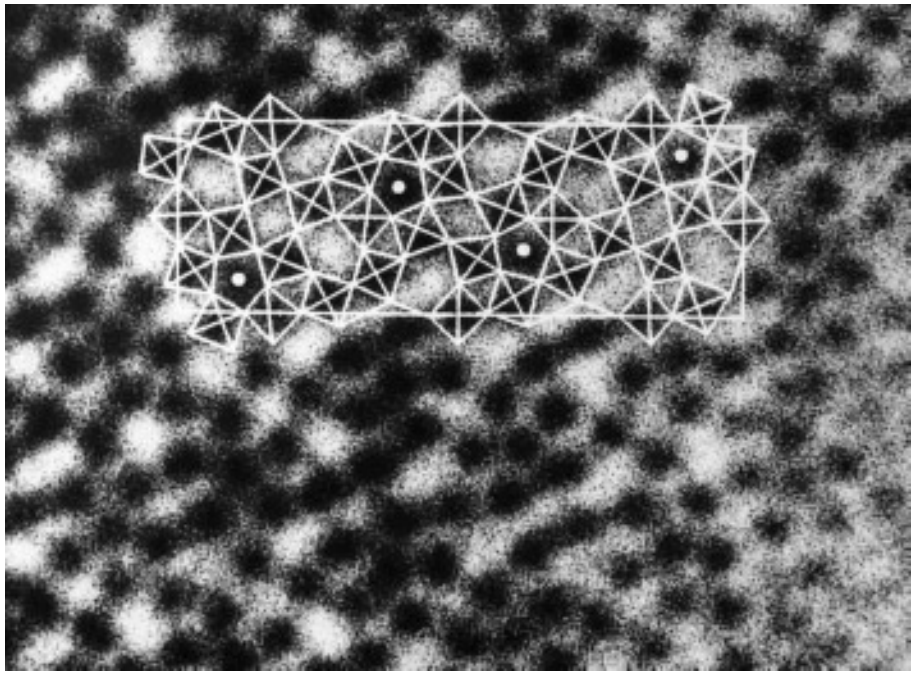

FIG. 3. Enlargement of a part of Fig. 2 with structural model of $Ta_8W_9O_{47}$ (T = 1400°C) embedded into the HRTEM image.

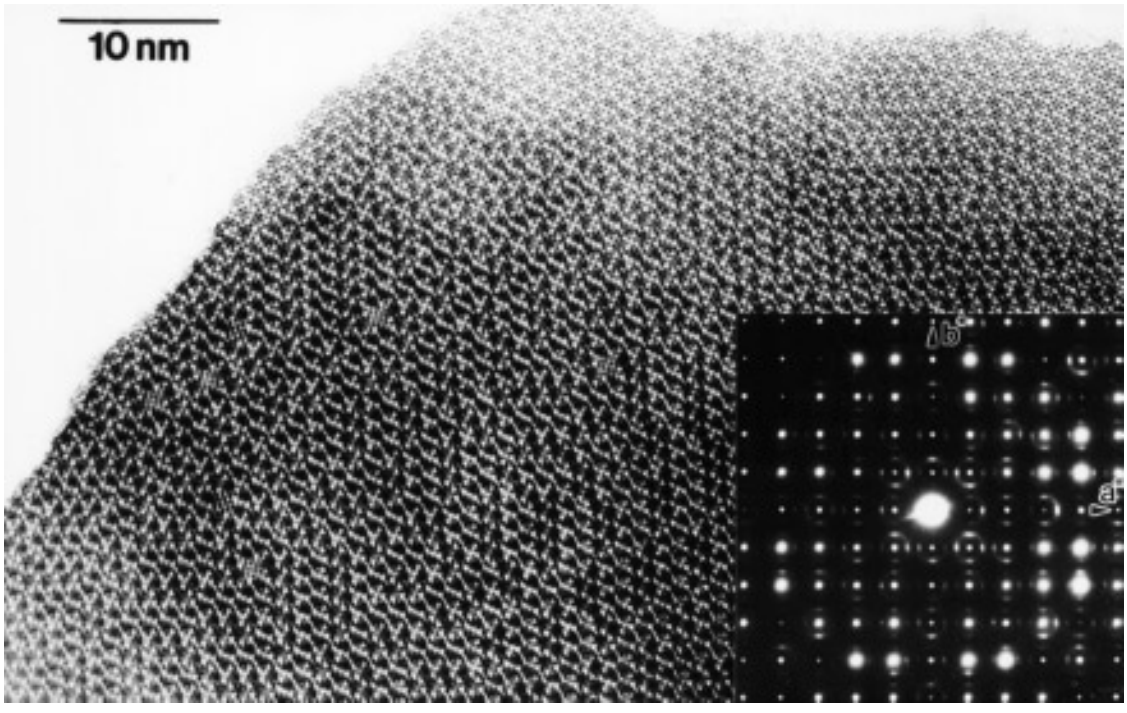

FIG. 4. $Ta_8W_9O_{47}$ (T = 1200°C): HRTEM image and electron diffraction pattern along [001].

shares edges with two square-shaped tunnels so that each type of pentagons can be only a part in chains along either [110] or [−110] directions of the TTB subcell. The diffractogram (Fig. 5b) of this image exhibits the circular diffuse scattering as it appears also in the electron diffraction pattern.

The origin of the diffuse scattering can be demonstrated in a highly disordered crystal region. Such a disordered region is characterized by the weakness of the aforementioned superstructure reflections along the tetragonal axes in the diffractogram (Fig. 5b); i.e., this crystal area contains less regions with well-ordered high-temperature structure

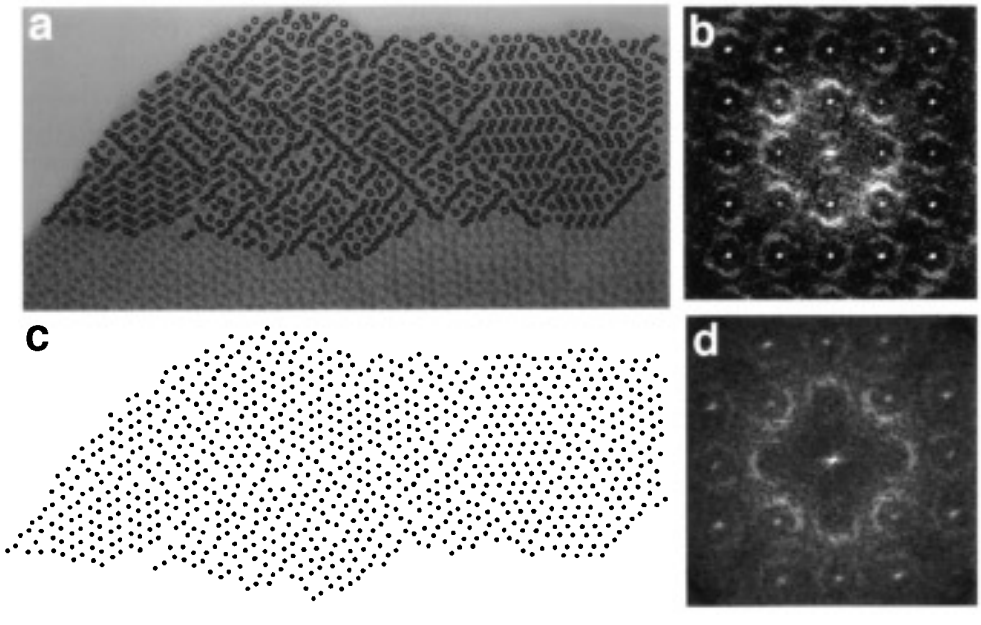

FIG. 5. (a) HRTEM image (Fig. 4) with the PCs outlined, (b) diffractogram of the HRTEM image, (c) point pattern representing the PC arrangement, and (d) diffractogram of the point pattern.

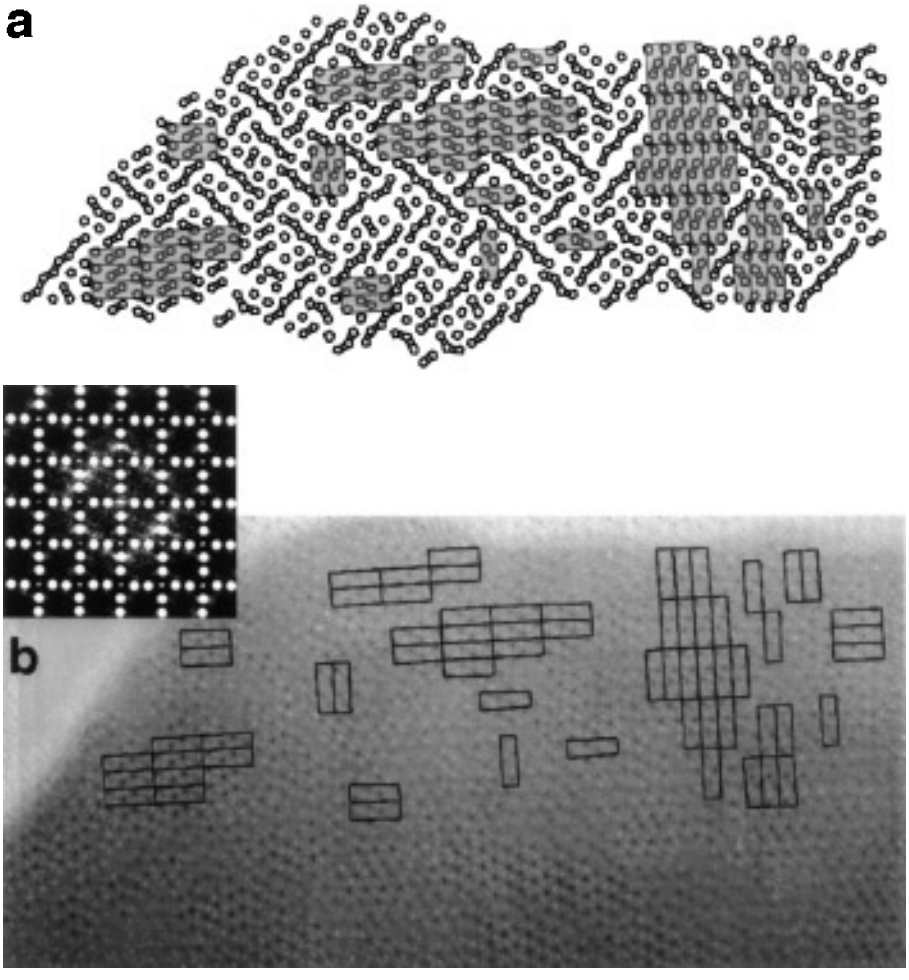

FIG. 6. (a) Representation of the PC arrangement of Fig. 5a with complete unit cells of threefold TTB-type structure outlined. The inset shows the diffractogram of the HRTEM image with a filter superposed allowing *only* the superstructure reflections to pass. (b) Filtered image with complete unit cells of threefold TTB-type structure outlined. Black spots in (b) correspond to PCs in regions with the superstructure. Regions with no black spots correspond to low ordering.

than the larger crystal fragment from which the electron diffraction pattern was recorded.

For sorting out the reason of diffuse scattering, a simplified description of the structure is chosen (Fig. 5c): Each PC is represented by a filled circle, the basic TTB framework is excluded. The Fourier transform of this point pattern gives the diffractogram shown in Fig. 5d being very similar to that obtained from the observed crystal area. In both cases, circular diffuse scattering occurs around the main reflections with the same radius ($\frac{1}{3}$ $\langle 100 \rangle^*$) as observed in the electron diffraction pattern. The circular diffuse scattering is, therefore, related to the disordered distribution of PCs whereas the microdomains of threefold TTB structure cause the superstructure reflections along the axes. This is supported by a filtered image (Fig. 6b) using only these superstructure reflections. The filtered image, which emphasizes ordered regions, reveals small areas of the threefold TTB structure which are spread over the whole crystal area. Their distribution coincides with the plot shown in Fig. 6a, i.e., the black spots occur at the positions of the PCs. However, besides the drawn PCs located inside the indicated regions with the threefold TTB-type superstructure, there are also other black spots in the filtered image. This is not surprising since on several sites the occupation of the pentagonal tunnels in one or two more TTB subunits is the same as in the threefold superstructure so that the determination of the origin of the unit cell in the ordered microdomains is ambiguous there. The areas with the threefold TTB-type superstructure are too small to be detected by X-ray methods so that only the TTB-type framework is found.

Furthermore, the TTB-type matrix structure is less ordered compared with the ideal structure observed at the higher processing temperature. There are 3×3 square

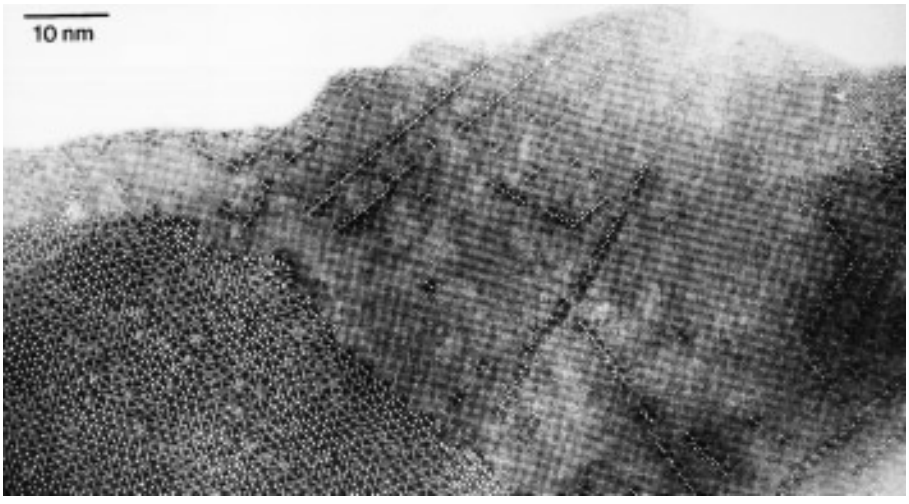

FIG. 7. HRTEM image of a tungsten-rich crystal region.

arrangements of bright dots recognizable in the TTB-type matrix (Fig. 4). They correspond to small areas of ReO_3-type structure (edge-sharing octahedra). Together with adjacent structural elements of the TTB-type structure, they represent single columns of $Ta_4W_7O_{31}$ units (4). Since this phase contains an higher amount of tungsten (Ta/W = 4/7) compared to the present phase (Ta/W = 8/9), local inhomogeneities concerning the cation distribution are likely.

Defects in a Tungsten-Rich Crystal Region

Besides the disorder, discussed above, some crystal areas have been observed in which the reaction between the binary oxides Ta_2O_5 and WO_3 is locally incomplete leading to a tungsten-rich region (Fig. 7) which has been shown by EDX analysis. There, the ReO_3-type structure of WO_3 is predominant. In the ReO_3-type matrix, several TTB-type cells are embedded. Some are isolated but most of them are arranged in chains (Fig. 8a). In this case, the connection between the TTB-type units is interesting: Two five-membered rings of octahedra have two octahedra in common so that they share an edge. Such double pentagons have been found before in defects in the CS structure of $(Nb,W)O_{2,95}$ (3). An enlargement of a region with a chain of TTB units is shown in Fig. 8a. There are two possible orientations for forming the double pentagons since each pentagon of octahedra has two edges for a connection (arrowed in Fig. 8a). Six TTB-type units are connected to form a straight chain (denoted as connection type A) but a bending occurs (right side of Fig. 8a) caused by two units which are connected in the alternative way (connection type B).

It can be seen that the TTB-type units are coherently embedded into the ReO_3-type structure. The perfect fit of the two lattices arises because a 4 × 4 block of corner-sharing octahedra corresponds in size to the TTB cell. Geometrically, the octahedra arrangement in the TTB cell can be derived from a 4 × 4 block of octahedra by rotating the central four octahedra by 45° (26). In

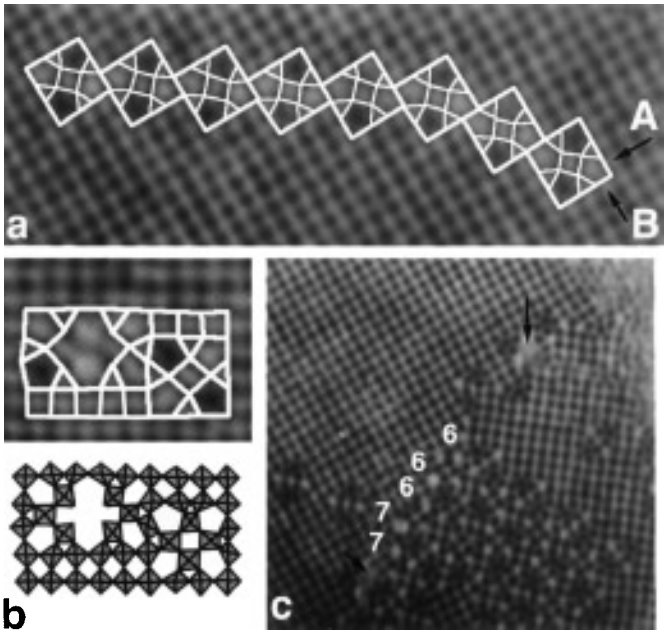

FIG. 8. Enlargement of defects in the crystal area shown in Fig. 7. (a) Two possibilities of forming a chain of TTB units are present (denoted as connection types A and B). (b) Arrangement of two fused TTB-type units. (c) The boundaries between two orientations of the ReO_3- type and between ReO_3- and TTB-type structures are disordered. Hexagonal (labeled 6) and heptagonal tunnels (labeled 7) occur. Areas exhibiting blurred contrast are indicated by arrows.

Fig. 8b, a different arrangement is present adjacent to a TTB-type unit. It corresponds in size to a 4×6 block of octahedra. Formally, two neighboring TTB-type units are fused so that two pentagonal tunnels are modified. The resulting structure is not unambiguously recognizable from the image.

The boundaries between areas of ReO_3-type structure with different orientations and of ReO_3- and TTB-type regions contain a lot of defects (Fig. 8c). Hexagonal and heptagonal tunnels can be seen. At several sites, indicated by arrows in Fig. 8c, the structure cannot be characterized from the HRTEM image so that disorder in the direction of view might be present.

4. CONCLUSIONS

$Ta_8W_9O_{47}$ crystallizes in structures closely related to the TTB type. The basic octahedra framework is the same for both the low- and high-temperature products, but different kinds of ordering of the PCs appear. The undisturbed threefold TTB-type superstructure, which is isostructural to $Nb_8W_9O_{47}$ (14), is formed at the higher temperature (T = 1400°C, 120 h). Lower reaction temperature (T = 1200°C) and shorter reaction time (60 h) lead to a metastable non-equilibrium product with a less ordered structure. X-ray diffraction, giving only averaged structural information, can only detect the TTB-type part of this structure. The results of electron diffraction and HRTEM investigations show that a rather disordered distribution of PCs is present instead. The threefold TTB-type superstructure is found only in small microdomains. On the other side, it is remarkable that deviating structures in the PC sublattice occur. Locally, chains of diamond linked PCs up to nine elements long are present. This arrangement appears to be thermodynamically favored compared to a totally statistical distribution of PCs.

It has been shown by Fourier analysis that for T = 1200°C the amount of disorder in the PC sublattice causes circular diffuse scattering in the electron diffraction pattern. The tetragonal metric of tantalum tungsten oxides found for other compositions in this range is probably also caused by a disordered distribution of the PCs.

REFERENCES

1. T. Ekström and R. J. D. Tilley, *J. Solid State Chem.* **18,** 123 (1976).
2. P. J. England, J. Booth, R. J. D. Tilley, and T. Ekström, *J. Solid State Chem.* **44,** 60 (1982).
3. P. J. England and R. J. D. Tilley, *Chem. Scr.* **20,** 102 (1982).
4. P. J. England and R. J. D. Tilley, *Chem. Scr.* **23,** 15 (1984).
5. N. C. Stephenson and R. S. Roth, *Acta Crystallogr. Sect. B* **27,** 1010, 1018, 1025, 1031 (1971).
6. S. Schmid, R. L. Withers, and J. G. Thompson, *J. Solid State Chem.* **99,** 226 (1992).
7. T. Miyano and K. Kosuge, *Eur. J. Solid State Inorg. Chem.* **31,** 867 (1994).
8. S. Schmid, J. G. Thompson, A. D. Rae, B. D. Butler, and R. L. Withers, *Acta Crystallogr., Sect. B* **51,** 698 (1995)
9. A. D. Rae, S. Schmid, J. G. Thompson, and R. L. Withers, *Acta Crystallogr., Sect. B* **51,** 709 (1995)
10. N. C. Stephenson and R. S. Roth, *Acta Crystallogr. Sect. B* **27,** 1037 (1971).
11. A. Santaro, R. S. Roth, and D. Minor, *Acta Crystallogr. Sect. B* **35,** 1202 (1979).
12. M. Lundberg, *Acta Chem. Scand.* **19,** 2274 (1965).
13. D. Groult, C. Michel, and B. Raveau, *J. Inorg. Nucl. Chem.* **36,** 61 (1974).
14. A. W. Sleight, *Acta Chem. Scand.* **20,** 1102 (1966).
15. B. O. Marinder, *Angew. Chem. Int. Ed. Engl.* **25,** 431 (1986).
16. L. Eyring and L.-T. Tai, in "Treatise on Solid State Chemistry" (N. B. Hannay, Ed.), Vol. 3, p. 167. Plenum, New York, 1976.
17. R. de Ridder, G. van Tendeloo, D. van Dyck, and S. Amelinckx, *Phys. Status Solidi. A* **41,** 555 (1977).
18. S. Iijima and J. M. Cowley, *J. Phys. Colloq.* **38**(C7), 135 (1977).
19. S. Horiuchi, K. Muramatsu, and Y. Matsui, *J. Appl. Crystallogr.* **13,** 141 (1980).
20. E. Holcombe and D. D. Smith, *J. Am. Cer. Soc.* **61,** 163 (1978).
21. C. Michel, D. Groult, A. Deschanvres, and B. Raveau, *J. Inorg. Nucl. Chem.* **37,** 251 (1975).
22. J. C. H. Spence, "Experimental High Resolution Electron Microscopy," 2nd ed., Oxford Univ. Press, London, 1988.
23. S. Horiuchi, K. Muramatsu, and Y. Matsui, *Acta Crystallogr. Sect. A* **34,** 939 (1978).
24. F. Krumeich, A. Hussain, C. Bartsch, and R. Gruehn, *Z. Anorg. Allg. Chem.* **621,** 799 (1995).
25. M. Lundberg, M. Sundberg, and A. Magnéli, *J. Solid State Chem.* **44,** 32 (1982).
26. B. G. Hyde and M. O'Keeffe, *Acta Crystallogr. Sect. A* **29,** 243 (1973).